
Temporal Spike Sequence Learning via Backpropagation for Deep Spiking Neural Networks

Wenrui Zhang

University of California, Santa Barbara
Santa Barbara, CA 93106
wenruizhang@ucsb.edu

Peng Li

University of California, Santa Barbara
Santa Barbara, CA 93106
lip@ucsb.edu

Abstract

Spiking neural networks (SNNs) are well suited for spatio-temporal learning and implementations on energy-efficient event-driven neuromorphic processors. However, existing SNN error backpropagation (BP) methods lack proper handling of spiking discontinuities and suffer from low performance compared with the BP methods for traditional artificial neural networks. In addition, a large number of time steps are typically required to achieve decent performance, leading to high latency and rendering spike based computation unscalable to deep architectures. We present a novel Temporal Spike Sequence Learning Backpropagation (TSSL-BP) method for training deep SNNs, which breaks down error backpropagation across two types of inter-neuron and intra-neuron dependencies and leads to improved temporal learning precision. It captures inter-neuron dependencies through presynaptic firing times by considering the all-or-none characteristics of firing activities, and captures intra-neuron dependencies by handling the internal evolution of each neuronal state in time. TSSL-BP efficiently trains deep SNNs within a much shortened temporal window of a few steps while improving the accuracy for various image classification datasets including CIFAR10.

1 Introduction

Spiking neural networks (SNNs), a brain-inspired computational model, have gathered significant interests [9]. The spike-based operational principles of SNNs not only allow information coding based on efficient temporal codes and give rise to promising spatiotemporal computing power but also render energy-efficient VLSI neuromorphic chips such as IBM's TrueNorth [1] and Intel's Loihi [6]. Despite the recent progress in SNNs and neuromorphic processor designs, fully leveraging the theoretical computing advantages of SNNs over traditional artificial neural networks (ANNs) [17] to achieve competitive performance in wide ranges of challenging real-world tasks remains difficult.

Inspired by the success of error backpropagation (BP) and its variants in training conventional deep neural networks (DNNs), various SNNs BP methods have emerged, aiming at attaining the same level of performance [4, 16, 24, 13, 21, 28, 11, 2, 3, 29]. Although many appealing results are achieved by these methods, developing SNNs BP training methods that are on a par with the mature BP tools widely available for training ANNs today is a nontrivial problem [22].

Training of SNNs via BP are challenged by two fundamental issues. First, from an algorithmic perspective, the complex neural dynamics in both spatial and temporal domains make the BP process obscure. Moreover, the errors are hard to be precisely backpropagated due to the non-differentiability of discrete spike events. Second, a large number of time steps are typically required for emulating SNNs in time to achieve decent performance, leading to high latency and rendering spike based computation unscalable to deep architectures. It is desirable to demonstrate the success of BP in training deeper SNNs achieving satisfactory performances on more challenging datasets. We propose a

new SNNs BP method, called temporal spike sequence learning via BP (TSSL-BP), to learn any target output temporal spiking sequences. TSSL-BP acts as a universal training method for any employed spike codes (rate, temporal, and combinations thereof). To tackle the above difficulties, TSSL-BP breaks down error backpropagation across two types of inter-neuron and intra-neuron dependencies, leading to improved temporal learning precision. It captures the inter-neuron dependencies within an SNN by considering the all-or-none characteristics of firing activities through presynaptic firing times; it considers the internal evolution of each neuronal state through time, capturing how the intra-neuron dependencies between different firing times of the same presynaptic neuron impact its postsynaptic neuron. The efficacy and precision of TSSL-BP allows it to successfully train SNNs over a very short temporal window, e.g. over 5-10 time steps, enabling ultra-low latency spike computation. As shown in Section 4, TSSL-BP significantly improves accuracy and runtime efficiency of BP training on several well-known image datasets of MNIST [15], NMNIST [19], FashionMNIST [26], and CIFAR10 [14]. Specifically, it achieves up to 3.98% accuracy improvement over the previously reported SNN work on CIFAR10, a challenging dataset for all prior SNNs BP methods.

2 Background

2.1 Existing Backpropagation methods for SNNs

One of the earliest SNNs BP methods is the well-known SpikeProp algorithm [4]. However, SpikeProp and its variants [5, 10, 27] are still limited to single spike per output neuron without demonstrating competitive performance on real-world tasks. In addition, [7, 8, 12, 20] train ANNs and then approximately convert them to SNNs. Nevertheless, such conversion leads to approximation errors and cannot exploit SNNs' temporal learning capability.

Recently, training SNNs with BP under a firing rate (or activity level) coded loss function has been shown to deliver competitive performances [16, 24, 21, 13, 28, 11, 2, 29]. Among them, [16] does not consider the temporal correlations of neural activities and treats spiking times as noise to allow error gradient computation. [21, 24, 28, 2] capture the temporal effects by performing backpropagation through time (BPTT) [23]. However, they get around the non-differentiability of spike events by approximating the spiking process using the surrogate gradient method [18]. These approximations lead to inconsistency between the computed gradient and target loss, and thus degrade training performance. [11] presents a BP method for recurrent SNNs based on a novel combination of a gate function and threshold-triggered synaptic model that are introduced to handle non-differentiability of spikes. In this work, depolarization of membrane potential within a narrow active zone below the firing threshold also induces graded postsynaptic current. [13, 29] present spike-train level BP methods by capturing the effects of spiking neurons aggregated at the spike train level. However, the length of spike trains over which BP is applied need to be long enough, leading to long inference latency and high training cost.

[25] can train SNNs over a relatively small number of time steps by adding optimization techniques such as neuron normalization and population decoding. Since its core lies at the method of [24], it still approximates the all-or-none firing characteristics of spiking neurons by a continuous activation function, causing the same problems introduced before.

In this work, we propose the TSSL-BP method as a universal training method for any employed spike codes. It can not only precisely capture the temporal dependencies but also allow ultra-low latency inference and training over only five time steps while achieving excellent accuracies.

2.2 Spiking Neuron Model

SNNs employ more biologically plausible spiking neuron models than ANNs. In this work, we adopt the leaky integrate-and-fire (LIF) neuron model and synaptic model [9].

Consider the input spike train from pre-synaptic neuron j to neuron i : $s_j(t) = \sum_{t_j^{(f)}} \delta(t - t_j^{(f)})$, where $t_j^{(f)}$ denotes a particular firing time of presynaptic neuron j . The incoming spikes are converted into an (unweighted) postsynaptic current (PSC) $a_j(t)$ through a synaptic model. The neuronal

membrane voltage $u_i(t)$ at time t for neuron i is given by

$$\tau_m \frac{du_i(t)}{dt} = -u_i(t) + R \sum_j w_{ij} a_j(t) + \eta_i(t), \quad (1)$$

where R and τ_m are the effective leaky resistance and time constant of the membrane, w_{ij} is the synaptic weight from pre-synaptic neuron j to neuron i , $a_j(t)$ is the (unweighted) postsynaptic potential (PSC) induced by the spikes from pre-synaptic neuron j , and $\eta(t)$ denotes the reset function.

The PSC and the reset function can be written as

$$a_j(t) = (\epsilon * s_j)(t), \quad \eta_i(t) = (\nu * s_i)(t), \quad (2)$$

where $\epsilon(\cdot)$ and $\nu(\cdot)$ are the spike response and reset kernel, respectively. In this work, we adopt a first order synaptic model as the spike response kernel which is expressed as:

$$\tau_s \frac{a_j(t)}{dt} = -a_j(t) + s_j(t), \quad (3)$$

where τ_s is the synaptic time constant.

The reset kernel reduces the membrane potential by a certain amount Δ_R , where Δ_R is equal to the firing threshold right after the neuron fires. Considering the discrete time steps simulation, we use the fixed-step first-order Euler method to discretize (1) to

$$u_i[t] = \left(1 - \frac{1}{\tau_m}\right) u_i[t-1] + \sum_j w_{ij} a_j[t] + \eta_i[t]. \quad (4)$$

The ratio of R and τ_m is absorbed into the synaptic weight. The reset function $\eta_i[t]$ represents the firing-and-resetting mechanism of the neuron model. Moreover, the firing output of the neuron is expressed as

$$s_i[t] = H(u_i[t] - V_{th}), \quad (5)$$

where V_{th} is the firing threshold and $H(\cdot)$ is the Heaviside step function.

3 Methods

3.1 Forward Pass

Without loss of generality, we consider performing BP across two adjacent layers $l-1$ and l with N_{l-1} and N_l neurons, respectively, in a fully-connected feedforward SNNs as shown in Figure 1. The procedure can be also applied to convolutional and pooling layers. Denote the presynaptic weights by $\mathbf{W}^{(l)} = [\mathbf{w}_1^{(l)}, \dots, \mathbf{w}_{N_l}^{(l)}]^T$,

where $\mathbf{w}_i^{(l)}$ is a column vector of weights from all the neurons in layer $l-1$ to the neuron i of layer l . In addition, we also denote PSCs from neurons in layer $l-1$ by $\mathbf{a}^{(l-1)}[t] = [a_1^{(l-1)}[t], \dots, a_{N_{l-1}}^{(l-1)}[t]]^T$, spike trains output

of the $l-1$ layer by $\mathbf{s}^{(l-1)}[t] = [s_1^{(l-1)}[t], \dots, s_{N_{l-1}}^{(l-1)}[t]]^T$, membrane potentials and the corresponding output spike trains of the l layer neurons respectively by $\mathbf{u}^{(l)}[t] = [u_1^{(l)}[t], \dots, u_{N_l}^{(l)}[t]]^T$ and $\mathbf{s}^{(l)}[t] = [s_1^{(l)}[t], \dots, s_{N_l}^{(l)}[t]]^T$, where variables associated with neurons in the layer l have l as the superscript.

The forward propagation between the two layers is described as

$$\begin{aligned} \mathbf{a}^{(l-1)}[t] &= (\epsilon * \mathbf{s}^{(l-1)}[t]), & \mathbf{u}^{(l)}[t] &= \left(1 - \frac{1}{\tau_m}\right) \mathbf{u}^{(l)}[t-1] + \mathbf{W}^{(l)} \mathbf{a}^{(l-1)}[t] + (\nu * \mathbf{s}^{(l)}[t]), \\ \mathbf{s}^{(l)}[t] &= H(\mathbf{u}^{(l)}[t] - V_{th}). \end{aligned} \quad (6)$$

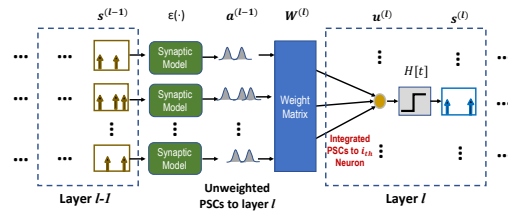


Figure 1: Forward evaluation pass of SNNs.

In the forward pass, the spike trains $\mathbf{s}^{(l-1)}[t]$ of the $l - 1$ layer generate the (unweighted) PSCs $\mathbf{a}^{(l-1)}[t]$ according to the synaptic model. Then, $\mathbf{a}^{(l-1)}[t]$ are multiplied the synaptic weights and passed onto the neurons of layer l . The integrated PSCs alter the membrane potentials and trigger the output spikes of the layer l neurons when the membrane potentials exceed the threshold.

3.2 The Loss Function

The goal of the proposed TSSL-BP method is to train a given SNN in such a way that each output neuron learns to produce a desired firing sequence arbitrarily specified by the user according to the input class label. Denote the desired and the actual spike trains in the output layer by $\mathbf{d} = [\mathbf{d}[t_0], \dots, \mathbf{d}[t_{N_t}]]$ and $\mathbf{s} = [\mathbf{s}[t_0], \dots, \mathbf{s}[t_{N_t}]]$ where N_t is the number of the considered time steps, $\mathbf{d}[t]$ and $\mathbf{s}[t]$ the desired and actual firing events for all output neurons at time t , respectively.

The loss function L can be defined using any suitable distance function measuring the difference between \mathbf{d} and \mathbf{s} . In this work, the loss function is defined by the total square error summed over each output neuron at each time step:

$$L = \sum_{k=0}^{N_t} E[t_k] = \sum_{k=0}^{N_t} \frac{1}{2} ((\epsilon * \mathbf{d})[t_k] - (\epsilon * \mathbf{s})[t_k])^2, \quad (7)$$

where $E[t]$ is the error at time t and $\epsilon(\cdot)$ a kernel function which measures the so-called Van Rossum distance between the actual spike train and desired spike train.

3.3 Temporal Spike Sequence Learning via Backpropagation (TSSL-BP) Method

From the loss function (7), we define the error $E[t_k]$ at each time step. $E[t_k]$ is based on the output layer firing spikes at t_k which further depend on all neuron states $\mathbf{u}[t]$, $t \leq t_k$. Below we consider these temporal dependencies and derive the main steps of the proposed TSSL-BP method. Full details of the derivation are provided in Section 1 of the Supplementary Material.

Using (7) and the chain rule, we obtain

$$\frac{\partial L}{\partial \mathbf{W}^{(l)}} = \sum_{k=0}^{N_t} \sum_{m=0}^k \frac{\partial E[t_k]}{\partial \mathbf{u}^{(l)}[t_m]} \frac{\partial \mathbf{u}^{(l)}[t_m]}{\partial \mathbf{W}^{(l)}} = \sum_{m=0}^{N_t} \mathbf{a}^{(l-1)}[t_m] \sum_{k=m}^{N_t} \frac{\partial E[t_k]}{\partial \mathbf{u}^{(l)}[t_m]}. \quad (8)$$

Similar to the conventional backpropagation, we use δ to denote the back propagated error at time t_m as $\delta^{(l)}[t_m] = \sum_{k=m}^{N_t} \frac{\partial E[t_k]}{\partial \mathbf{u}^{(l)}[t_m]} \cdot \mathbf{a}^{(l-1)}[t_m]$ can be easily obtained from (6). $\delta^{(l)}[t_m]$ is considered in two cases.

[**l is the output layer.**] The $\delta^{(l)}[t_m]$ can be computed from

$$\delta^{(l)}[t_m] = \sum_{k=m}^{N_t} \frac{\partial E[t_k]}{\partial \mathbf{a}^{(l)}[t_k]} \frac{\partial \mathbf{a}^{(l)}[t_k]}{\partial \mathbf{u}^{(l)}[t_m]}. \quad (9)$$

The first term of (9) can be obtained directly from the loss function. The second term $\frac{\partial \mathbf{a}^{(l)}[t_k]}{\partial \mathbf{u}^{(l)}[t_m]}$ is the key part of the TSSL-BP method and is discussed in the following sections.

[**l is a hidden layer.**] $\delta^{(l)}[t_m]$ is derived using the chain rule and (6).

$$\delta^{(l)}[t_m] = \sum_{j=m}^{N_t} \sum_{k=m}^j \frac{\partial \mathbf{a}^{(l)}[t_k]}{\partial \mathbf{u}^{(l)}[t_m]} \left(\frac{\partial \mathbf{u}^{(l+1)}[t_k]}{\partial \mathbf{a}^{(l)}[t_k]} \frac{\partial E[t_j]}{\partial \mathbf{u}^{(l+1)}[t_k]} \right) = (\mathbf{W}^{(l+1)})^T \sum_{k=m}^{N_t} \frac{\partial \mathbf{a}^{(l)}[t_k]}{\partial \mathbf{u}^{(l)}[t_m]} \delta^{(l+1)}[t_k]. \quad (10)$$

(10) maps the error δ from layer $l + 1$ to layer l . It is obtained from the fact that membrane potentials $\mathbf{u}^{(l)}$ of the neurons in layer l influence their (unweighted) corresponding postsynaptic currents (PSCs) $\mathbf{a}^{(l)}$ through fired spikes, and $\mathbf{a}^{(l)}$ further affect the membrane potentials $\mathbf{u}^{(l+1)}$ in the next layer.

3.3.1 Key challenges in SNN BackPropagation

As shown above, for both the output layer and hidden layers, once $\frac{\partial \mathbf{a}^{(l)}[t_k]}{\partial \mathbf{u}^{(l)}[t_m]} (t_k \geq t_m)$ are known, the error δ can be back propagated and the gradient of each layer can be calculated.

Importantly, the dependencies of the PSCs on the corresponding membrane potentials of the presynaptic neurons reflected in $\frac{\partial a^{(l)}[t_k]}{\partial u^{(l)}[t_m]} (t_k \geq t_m)$ are due to the following spiking neural behaviors: a change in the membrane potential may bring it up to the firing threshold, and hence activate the corresponding neuron by generating a spike, which in turn produces a PSC. Computing $\frac{\partial a^{(l)}[t_k]}{\partial u^{(l)}[t_m]} (t_k \geq t_m)$ involves the activation of each neuron, i.e. firing a spike due to the membrane potential's crossing the firing threshold from below. Unfortunately, the all-or-none firing characteristics of spiking neurons makes the activation function nondifferentiable, introducing several key challenges.

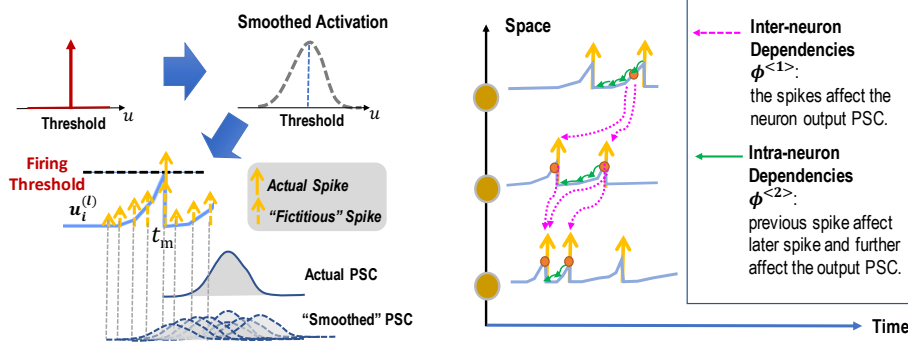


Figure 2: “Fictitious” smoothing of activation Figure 3: Inter/Intra neuron dependencies.

A typical strategy in dealing with the non-differentiability of the activation is to smooth the activation function by approximating it using a differentiable curve [24] as shown in the Figure 2, or a continuous probability density function [21], which is similar to the former approach in spirit. However, these approaches effectively spread each discrete firing spike continuously over time, converting one actual spike to multiple “fictitious” spikes and also generating multiple “fictitious” PSCs displaced at different time points. We stress that while smoothing circumvents the numerical challenges brought by non-differentiability of the spiking activation, it effectively alters the underlying spiking neuron model and firing times, and leads to degraded accuracy in the error gradient computation. It is important to reflect that spike timing is the hallmark of spiking neural computation, altering firing times in BP can hamper precise learning of the targeted firing sequences as pursued in this paper.

3.3.2 The Main Ideas Behind TSSL-BP

TSSL-BP addresses the two key limitations of the prior BP methods: lack proper handling of spiking discontinuities (leading to loss of temporal precision) and need for many time steps (i.e. high latency) to ensure good performance. TSSL-BP computes $\frac{\partial a^{(l)}[t_k]}{\partial u^{(l)}[t_m]}$ across two categories of spatio-temporal dependencies in the network: **inter-neuron** and **intra-neuron** dependencies. As shown in Figure 3, our key observations are: 1) temporal dependencies of a postsynaptic neuron on any of its presynaptic neurons *only* take place via the presynaptic spikes which generate PSCs to the postsynaptic neuron, and shall be considered as inter-neuron dependencies; 2) furthermore, the timing of one presynaptic spike affects the timing of the immediately succeeding spike from the same presynaptic neuron through the intra-neuron temporal dependency. The timing of the first presynaptic spike affects the PSC produced by the second spike, and has additional impact on the postsynaptic neuron through this indirect mechanism. In the following, we show how to derive the $\frac{\partial a_i^{(l)}[t_k]}{\partial u_i^{(l)}[t_m]}$ for each neuron i in layer l . We denote $\phi_i^{(l)}(t_k, t_m) = \frac{\partial a_i^{(l)}[t_k]}{\partial u_i^{(l)}[t_m]} = \phi_i^{(l)<1>}(t_k, t_m) + \phi_i^{(l)<2>}(t_k, t_m)$, where $\phi_i^{(l)<1>}(t_k, t_m)$ represents the inter-neuron dependencies and $\phi_i^{(l)<2>}(t_k, t_m)$ is the intra-neuron dependencies.

3.3.3 Inter-Neuron Backpropagation

Instead of performing the problematic activation smoothing, we critically note that the all-or-none characteristics of firing behavior is such that a PSC waveform is only triggered at a presynaptic firing time. Specially, as shown in Figure 4, a perturbation $\Delta u_i^{(l)}$ of $u_i^{(l)}[t_m]$, i.e. due to weight updates, may result in an incremental shift in the firing time Δt , which in turn shifts the onset of the PSC

waveform corresponding to the shifted spike, leading to a perturbation $\Delta a_i^{(l)}$ of $a_i^{(l)}[t_k]$. We consider this as an inter-neuron dependency since the change in PSC ($\Delta a_i^{(l)}$) alters the membrane potential of the postsynaptic neuron in the next layer.

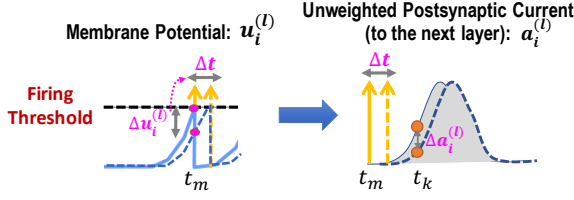


Figure 4: PSC dependencies on presynaptic potential.

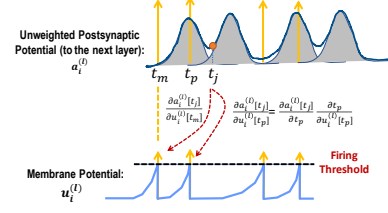


Figure 5: Inter-neuron dependencies.

We make two important points: 1) we shall capture the inter-neuron dependencies via (the incremental changes of) the presynaptic firing times, which precisely corresponds to how different neurons interact with each other in an SNN; and 2) the *inter-neuron* dependency of each neuron i 's PSC $a_i^{(l)}$ at t_k on its membrane potential $u_i^{(l)}$ at t_m happens only if the neuron fires at t_m . In general, $a_i^{(l)}[t_k]$'s inter-neuron dependencies on *all* preceding firing times shall be considered. Figure 5 shows the situation where $a_i^{(l)}[t_k]$ depends on two presynaptic firing times t_m and t_p . Conversely, the inter-neuron dependencies $\phi_i^{(l)<1>}(t_k, t_m) = 0$ if $t_k < t_m$ or there is no spike at t_m . Assuming that the presynaptic neuron i spikes at t_m , The inter-neuron dependencies is

$$\phi_i^{(l)<1>}(t_k, t_m) = \frac{\partial a_i^{(l)}[t_k]}{\partial t_m} \frac{\partial t_m}{\partial u_i^{(l)}[t_m]}, \quad (11)$$

where, importantly, the chain rule is applied through the presynaptic firing time t_m .

From (2), the two parts part of (11) can be calculated as

$$\frac{\partial a_i^{(l)}[t_k]}{\partial t_m} = \frac{\partial(\epsilon * s_i^{(l)}[t_m])[t_k]}{\partial t_m}, \quad \frac{\partial t_m}{\partial u_i^{(l)}[t_m]} = \frac{-1}{\frac{\partial u_i^{(l)}[t_m]}{\partial t_m}}, \quad (12)$$

where $\frac{\partial u_i^{(l)}[t_m]}{\partial t_m}$ is obtained by differentiating (4).

3.3.4 Intra-Neuron Backpropagation

Now we consider the intra-neuron dependency $\phi_i^{(l)<2>}(t_k, t_m)$ defined between an arbitrary time t_k and a presynaptic firing time t_m ($t_m < t_k$). From Section 3.3.3, the presynaptic firing at time t_m invokes a continuous PSC which has a direct impact on the postsynaptic potential at time t_k , which is an inter-neuron dependency. On the other hand, $\phi_i^{(l)<2>}(t_k, t_m)$ corresponds to an indirect effect on the postsynaptic potential via the intra-neuron dependency.

We consider $\phi_i^{(l)<2>}(t_k, t_m)$ specifically under the context of the adopted LIF model, which may occur if the presynaptic neuron spikes at t_p immediately following t_m such that $t_m < t_p < t_k$. In this case, the presynaptic membrane potential at t_m not only contributes to a PSC due to the neuron firing, but also affects the membrane potential at the next spike time t_p resulted from the reset occurring at t_m as described in (4). The PSC $a_i^{(l)}[t_k]$ has an inter-neuron dependency on membrane potential $u_i^{(l)}[t_p]$ while $u_i^{(l)}[t_p]$ is further affected by the immediately preceding firing time t_m due to the reset of the presynaptic potential at t_m . Recall $s_i^{(l)}[t] = 1$ if neuron i fires at t as in (5). More precisely, $\phi_i^{(l)<2>}(t_k, t_m)$ takes this indirect intra-neuron effect on $a_i^{(l)}[t_k]$ into consideration if

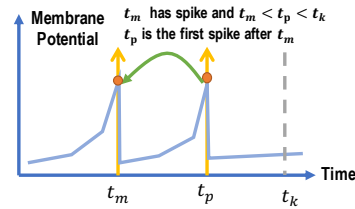


Figure 6: Intra-neuron dependencies.

$\exists t_p \in (t_m, t_k)$ such that $s_i^{(l)}[t_p] = 1$ and $s_i^{(l)}[t] = 0 \forall t \in (t_m, t_p)$, i.e. no other presynaptic spike exists between t_m and t_p

$$\phi_i^{(l)<2>}(t_k, t_m) = \frac{\partial a_i^{(l)}[t_k]}{\partial u_i^{(l)}[t_p]} \frac{\partial u_i^{(l)}[t_p]}{\partial t_m} \frac{\partial t_m}{\partial u_i^{(l)}[t_m]} = \phi_i^{(l)}(t_k, t_p) \frac{\partial(\nu * s_i^{(l)}[t_m])[t_p]}{\partial t_m} \frac{\partial t_m}{\partial u_i^{(l)}[t_m]}, \quad (13)$$

where $\nu(\cdot)$ is the reset kernel and $\frac{\partial t_m}{\partial u_i^{(l)}[t_m]}$ is evaluated by (12). In (13), $\phi_i^{(l)}(t_k, t_p)$ would have been already computed during the backpropagation process since t_p is a presynaptic firing time after t_m . Putting the inter-neuron and intra-neuron dependencies together, one of the key derivatives required in the BP process $\phi_i^{(l)}(t_k, t_m) = \frac{\partial a_i^{(l)}[t_k]}{\partial u_i^{(l)}[t_m]}$ with $t_m < t_p < t_k$ is given by

$$\phi_i^{(l)}(t_k, t_m) = \begin{cases} 0 & s_i^{(l)}[t_m] = 0, s_i^{(l)}[t_p] = 0 \forall t_p \in (t_m, t_k), \\ \frac{\partial a_i^{(l)}[t_k]}{\partial t_m} \frac{\partial t_m}{\partial u_i^{(l)}[t_m]} & s_i^{(l)}[t_m] = 1, s_i^{(l)}[t_p] = 0 \forall t_p \in (t_m, t_k), \\ \frac{\partial a_i^{(l)}[t_k]}{\partial t_m} \frac{\partial t_m}{\partial u_i^{(l)}[t_m]} + \phi_i^{(l)<2>}(t_k, t_m) & s_i^{(l)}[t_m] = 1, s_i^{(l)}[t_p] = 1, s_i^{(l)}[t] = 0 \forall t \in (t_m, t_p), \end{cases} \quad (14)$$

where t_p is an arbitrary time between t_m and t_k , and $\phi_i^{(l)<2>}(t_k, t_m)$ of (13) is considered.

The complete derivation of TSSL-BP is provided in Section 1 of the Supplementary Material. There are two key distinctions setting our approach apart from the aforementioned activation smoothing. First, the inter-neuron dependencies are only considered at pre-synaptic firing times as opposed to all prior time points, latter of which is the case when the activation smoothing is applied with BPTT. The handling adopted in TSSL-BP is a manifestation of the all-or-none firing characteristics of spiking neurons. Second, as in Figure 4, the key step in backpropagation is the consideration of the incremental change of spiking times, which is not considered in recent SNNs BP works.

4 Experiments and Results

We test the proposed TSSL-BP method on four image datasets MNIST [15], N-MNIST [19], Fashion-MNIST [26] and CIFAR10 [14]. We compare TSSL-BP with several state-of-the-art results with the same or similar network sizes including different SNNs BP methods, converted SNNs, and traditional ANNs. The details of practical simulation issues, experimental settings, and datasets preprocessing methods are described in Section 2 of the supplementary material. We have made our Pytorch implementation available online¹. We expect this work would help move the community forward towards enabling high-performance spiking neural networks simulation within short latency.

4.1 MNIST

On MNIST [15], we compares the accuracies of the spiking CNNs trained by the TSSL-BP method with ones trained by other algorithms in Table 1. In our method, the pixel intensities of the image are converted into real-valued spike current to the inputs within a short time window. The proposed TSSL-BP delivers up to 99.53% accuracy and outperforms all other methods except for the ST-RSBP [29] whose accuracy is slightly higher by 0.09%. However, compared to ST-RSBP, TSSL-BP can train high-performance SNNs with only 5 time steps, achieving $80\times$ reduction of step count (latency). The accuracy of [29] drops below that of TSSL-BP noticeably under short time windows. In addition, no data augmentation is applied in this experiment, which is adopted in [13] and [29].

4.2 N-MNIST

We test the proposed method on N-MNIST dataset [19], the neuromorphic version of the MNIST. The inputs to the networks are spikes rather than real value currents. Table 2 compares the results obtained by different models on N-MNIST. The SNN trained by our proposed approach naturally processes spatio-temporal spike patterns, achieving the start-of-the-art accuracy of 99.40%. It is important to note that our proposed method with the accuracy of 99.28% outperforms the best previously reported results in [21], obtaining 10 times fewer time steps which leads to significant latency reduction.

¹<https://github.com/stonezwr/TSSL-BP>

Table 1: Performances of Spiking CNNs on MNIST.

Methods	Network	Time steps	Epochs	Mean	Stddev	Best
Spiking CNN [16]	20C5-P2-50C5-P2-200	> 200	150			99.31%
STBP [24]	15C5-P2-40C5-P2-300	> 100	200			99.42%
SLAYER [21]	12C5-p2-64C5-p2	300	100	99.36%	0.05%	99.41%
HM2BP [13]	15C5-P2-40C5-P2-300	400	100	99.42%	0.11%	99.49%
ST-RSBP [29]	15C5-P2-40C5-P2-300	400	100	99.57%	0.04%	99.62%
This work	15C5-P2-40C5-P2-300	5	100	99.50%	0.02%	99.53%

20C5: convolution layer with 20 of the 5×5 filters. P2: pooling layer with 2×2 filters.

Table 2: Performances on N-MNIST.

Methods	Network	Time steps	Mean	Stddev	Best	Steps reduction
HM2BP [13]	400 – 400	600	98.88%	0.02%	98.88%	20x
SLAYER [21]	500 – 500	300	98.89%	0.06%	98.95%	10x
SLAYER [21]	12C5-P2-64C5-P2	300	99.20%	0.02%	99.22%	10x
This work	12C5-P2-64C5-P2	100	99.35%	0.03%	99.40%	3.3x
This work	12C5-P2-64C5-P2	30	99.23%	0.05%	99.28%	

All the experiments in this table train the N-MNIST for 100 epochs

4.3 FashionMNIST

We compare several trained fully-connected feedforward SNNs and spiking CNNs on FashionMNIST [26], a more challenging dataset than MNIST. In Table 3, TSSL-BP achieves 89.80% test accuracy on the fully-connected feedforward network of two hidden layers with each having 400 neurons, outperforming the HM2BP method of [13], which is the best previously reported algorithm for feedforward SNNs. TSSL-BP can also deliver the best test accuracy with much fewer time steps. Moreover, TSSL-BP achieves **92.83%** on the spiking CNN networks, noticeably outperforming the same size non-spiking CNN trained by a standard BP method.

Table 3: Performances on FashionMNIST.

Methods	Network	Time steps	Epochs	Mean	Stddev	Best
ANN [29]	400 – 400		100			89.01%
HM2BP [29]	400 – 400	400	100			88.99%
This work	400 – 400	5	100	89.75%	0.03%	89.80%
ANN [26]	32C5-P2-64C5-P2-1024		100			91.60%
This work	32C5-P2-64C5-P2-1024	5	100	92.69%	0.09%	92.83%

4.4 CIFAR10

Furthermore, we apply the proposed method on the more challenging dataset of CIFAR10 [14]. As shown in Table 4, our TSSL-BP method achieves 89.22% accuracy with a mean of 88.98% and a standard deviation of 0.27% under five trials on the first CNN and achieves 91.41% accuracy on the second CNN architecture. TSSL-BP delivers the best result among a previously reported ANN, SNNs converted from pre-trained ANNs, and the spiking CNNs trained by the STBP method of [25]. CIFAR10 is a challenging dataset for most of the existing SNNs BP methods since the long latency required by those methods makes them hard to scale to deeper networks. The proposed TSSL-BP not only achieves up to 3.98% accuracy improvement over the work of [25] without the additional optimization techniques including neuron normalization and population decoding which are employed in [25], but also utilizes fewer time steps.

Table 4: Performances of CNNs on CIFAR10.

Methods	Network	Time steps	Epochs	Accuracy
Converted SNN [12]	CNN 1	80		83.52%
STBP [25]	CNN 1	8	150	85.24%
This work	CNN 1	5	150	89.22%
ANN [25]	CNN 2			90.49%
Converted SNN [20]	CNN 2		200	87.46%
STBP (without NeuNorm) [25]	CNN 2	8	150	89.83%
STBP (with NeuNorm) [25]	CNN 2	8	150	90.53%
This work	CNN 2	5	150	91.41%

CNN 1: 96C3-256C3-P2-384C3-P2-384C3-256C3-1024-1024
 CNN 2: 128C3-256C3-P2-512C3-P2-1024C3-512C3-1024-512

4.5 Firing Sparsity

As presented, the proposed TSSL-BP method can train SNNs with low latency. In the meanwhile, the firing activities in well-trained networks also tend to be sparse. To demonstrate firing sparsity, we select two well-trained SNNs, one for the CIFAR10 and the other for the N-MNIST.

The CIFAR10 network is simulated over 5 time steps. We count the percentage of neurons that fire 0, 1, . . . , 5 times, respectively, and average the percentages over 100 testing samples. As shown in Figure 7, the network’s firing activity is sparse. More than 84% of neurons are silent while 12% of neurons fire more than once, and about 4% of neurons fire at every time step.

The N-MNIST network demonstrated here is simulated over 100 time steps. The firing rate of each neuron is logged. The number of neurons with a certain range of firing rates is counted and averaged over 100 testing samples. Similarly, as shown in Figure 8, the firing events of the N-MNIST network are also sparse and more than 75% of neurons keep silent. In the meanwhile, there are about 5% of neurons with a firing rate of greater than 10%.

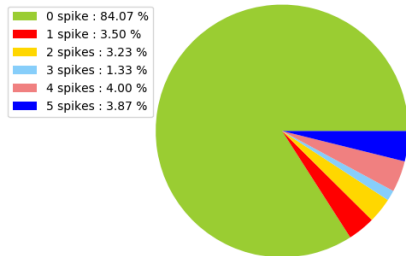


Figure 7: Firing activity on CIFAR10

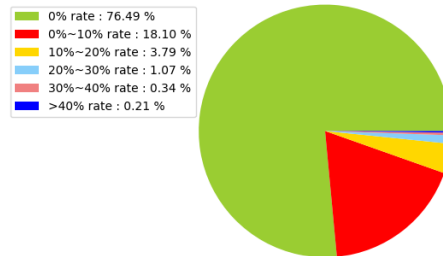


Figure 8: Firing activity on N-MNIST

5 Conclusion

We have presented the novel temporal spike sequence learning via a backpropagation (TSSL-BP) method to train deep SNNs. Unlike all prior SNNs BP methods, TSSL-BP improves temporal learning precision by circumventing the non-differentiability of the spiking activation function while faithfully reflecting the all-or-none firing characteristics and the underlying structure in the dependencies of spiking neural activities in both space and time.

TSSL-BP provides a universal BP tool for learning arbitrarily specified target firing sequences with high accuracy while achieving low temporal latency. This is in contrast with most of the existing SNN BP methods which require hundreds of time steps for achieving decent accuracy. The ability in training and inference over a few time steps results in significant reductions of the computational cost required for training large/deep SNNs, and the decision time and energy dissipation of the SNN model when deployed on either a general-purpose or a dedicated neuromorphic computing platform.

Broader Impact

Our proposed Temporal Spike Sequence Learning Backpropagation (TSSL-BP) method is able to train deep SNNs while achieving the state-of-the-art efficiency and accuracy. TSSL-BP breaks down error backpropagation across two types of inter-neuron and intra-neuron dependencies and leads to improved temporal learning precision. It captures inter-neuron dependencies through presynaptic firing times by considering the all-or-none characteristics of firing activities, and captures intra-neuron dependencies by handling the internal evolution of each neuronal state in time.

Spiking neural networks offer a very appealing biologically plausible model of computation and may give rise to ultra-low power inference and training on recently emerged large-scale neuromorphic computing hardware. Due to the difficulties in dealing with the all-or-one characteristics of spiking neurons, however, training of SNNs is a major present challenge and has limited wide adoption of SNNs models.

The potential impacts of this work are several-fold:

- 1) **Precision:** TSSL-BP offers superior precision in learning arbitrarily specified target temporal sequences, outperforming all recently developed the-state-of-the-art SNN BP methods.
- 2) **Low latency:** TSSL-BP delivers high-precision training over a very short temporal window of a few time steps. This is contrast with many BP methods that require hundreds of time steps for maintaining a decent accuracy. Low latency computation immediately corresponds to fast decision making.
- 3) **Scalability and energy efficiency:** The training of SNNs is significantly more costly than that of the conventional neural networks. The training cost is one major bottleneck to training large/deep SNNs in order to achieve competitive performance. The low latency training capability of TSSL-BP reduces the training cost by more than one order of magnitude and also cuts down the energy dissipation of the training and inference on the deployed computing hardware.
- 4) **Community impact:** TSSL-BP has been prototyped based on the widely adopted Pytorch framework and will be made available to the public. We believe our TSSL-BP code will benefit the brain-inspired computing community from both an algorithmic and neuromorphic computing hardware development perspective.

Acknowledgments

This material is based upon work supported by the National Science Foundation (NSF) under Grants No.1948201 and No.1940761. Any opinions, findings, conclusions or recommendations expressed in this material are those of the authors and do not necessarily reflect the views of NSF, UC Santa Barbara, and their contractors.

References

- [1] Filipp Akopyan, Jun Sawada, Andrew Cassidy, Rodrigo Alvarez-Icaza, John Arthur, Paul Merolla, Nabil Imam, Yutaka Nakamura, Pallab Datta, Gi-Joon Nam, et al. Truenorth: Design and tool flow of a 65 mw 1 million neuron programmable neurosynaptic chip. *IEEE Transactions on Computer-Aided Design of Integrated Circuits and Systems*, 34(10):1537–1557, 2015.
- [2] Guillaume Bellec, Darjan Salaj, Anand Subramoney, Robert Legenstein, and Wolfgang Maass. Long short-term memory and learning-to-learn in networks of spiking neurons. In *Advances in Neural Information Processing Systems*, pages 787–797, 2018.
- [3] Guillaume Bellec, Franz Scherr, Elias Hajek, Darjan Salaj, Robert Legenstein, and Wolfgang Maass. Biologically inspired alternatives to backpropagation through time for learning in recurrent neural nets. *arXiv preprint arXiv:1901.09049*, 2019.
- [4] Sander M Bohte, Joost N Kok, and Han La Poutre. Error-backpropagation in temporally encoded networks of spiking neurons. *Neurocomputing*, 48(1-4):17–37, 2002.
- [5] Olaf Booiij and Hieu tat Nguyen. A gradient descent rule for spiking neurons emitting multiple spikes. *Information Processing Letters*, 95(6):552–558, 2005.

- [6] Mike Davies, Narayan Srinivasa, Tsung-Han Lin, Gautham Chinya, Yongqiang Cao, Sri Harsha Choday, Georgios Dimou, Prasad Joshi, Nabil Imam, Shweta Jain, et al. Loihi: A neuromorphic manycore processor with on-chip learning. *IEEE Micro*, 38(1):82–99, 2018.
- [7] Peter U Diehl, Daniel Neil, Jonathan Binas, Matthew Cook, Shih-Chii Liu, and Michael Pfeiffer. Fast-classifying, high-accuracy spiking deep networks through weight and threshold balancing. In *Neural Networks (IJCNN), 2015 International Joint Conference on*, pages 1–8. IEEE, 2015.
- [8] Steve K Esser, Rathinakumar Appuswamy, Paul Merolla, John V Arthur, and Dharmendra S Modha. Backpropagation for energy-efficient neuromorphic computing. In *Advances in Neural Information Processing Systems*, pages 1117–1125, 2015.
- [9] Wulfram Gerstner and Werner M Kistler. *Spiking neuron models: Single neurons, populations, plasticity*. Cambridge university press, 2002.
- [10] Samanwoy Ghosh-Dastidar and Hojjat Adeli. A new supervised learning algorithm for multiple spiking neural networks with application in epilepsy and seizure detection. *Neural networks*, 22(10):1419–1431, 2009.
- [11] Dongsung Huh and Terrence J Sejnowski. Gradient descent for spiking neural networks. In *Advances in Neural Information Processing Systems*, pages 1433–1443, 2018.
- [12] Eric Hunsberger and Chris Eliasmith. Training spiking deep networks for neuromorphic hardware. *arXiv preprint arXiv:1611.05141*, 2016.
- [13] Yingyezhe Jin, Wenrui Zhang, and Peng Li. Hybrid macro/micro level backpropagation for training deep spiking neural networks. In *Advances in Neural Information Processing Systems*, pages 7005–7015, 2018.
- [14] Alex Krizhevsky, Vinod Nair, and Geoffrey Hinton. The cifar-10 dataset. *online: <http://www.cs.toronto.edu/kriz/cifar.html>*, 2014.
- [15] Yann LeCun, Léon Bottou, Yoshua Bengio, and Patrick Haffner. Gradient-based learning applied to document recognition. *Proceedings of the IEEE*, 86(11):2278–2324, 1998.
- [16] Jun Haeng Lee, Tobi Delbruck, and Michael Pfeiffer. Training deep spiking neural networks using backpropagation. *Frontiers in neuroscience*, 10:508, 2016.
- [17] Wolfgang Maass. Networks of spiking neurons: the third generation of neural network models. *Neural networks*, 10(9):1659–1671, 1997.
- [18] EO Neftci, H Mostafa, and F Zenke. Surrogate gradient learning in spiking neural networks, 2019. URL <https://arxiv.org/abs>, 1901.
- [19] Garrick Orchard, Ajinkya Jayawant, Gregory K Cohen, and Nitish Thakor. Converting static image datasets to spiking neuromorphic datasets using saccades. *Frontiers in neuroscience*, 9:437, 2015.
- [20] Abhronil Sengupta, Yuting Ye, Robert Wang, Chiao Liu, and Kaushik Roy. Going deeper in spiking neural networks: Vgg and residual architectures. *Frontiers in neuroscience*, 13, 2019.
- [21] Sumit Bam Shrestha and Garrick Orchard. Slayer: Spike layer error reassignment in time. In *Advances in Neural Information Processing Systems*, pages 1412–1421, 2018.
- [22] Amirhossein Tavanaei, Masoud Ghodrati, Saeed Reza Kheradpisheh, Timothée Masquelier, and Anthony Maida. Deep learning in spiking neural networks. *Neural Networks*, 2018.
- [23] Paul J Werbos. Backpropagation through time: what it does and how to do it. *Proceedings of the IEEE*, 78(10):1550–1560, 1990.
- [24] Yujie Wu, Lei Deng, Guoqi Li, Jun Zhu, and Luping Shi. Spatio-temporal backpropagation for training high-performance spiking neural networks. *Frontiers in neuroscience*, 2018.

- [25] Yujie Wu, Lei Deng, Guoqi Li, Jun Zhu, Yuan Xie, and Luping Shi. Direct training for spiking neural networks: Faster, larger, better. In *Proceedings of the AAAI Conference on Artificial Intelligence*, volume 33, pages 1311–1318, 2019.
- [26] Han Xiao, Kashif Rasul, and Roland Vollgraf. Fashion-mnist: a novel image dataset for benchmarking machine learning algorithms. *arXiv preprint arXiv:1708.07747*, 2017.
- [27] Yan Xu, Xiaoqin Zeng, Lixin Han, and Jing Yang. A supervised multi-spike learning algorithm based on gradient descent for spiking neural networks. *Neural Networks*, 43:99–113, 2013.
- [28] Friedemann Zenke and Surya Ganguli. Superspike: Supervised learning in multilayer spiking neural networks. *Neural computation*, 30(6):1514–1541, 2018.
- [29] Wenrui Zhang and Peng Li. Spike-train level backpropagation for training deep recurrent spiking neural networks. In *Advances in Neural Information Processing Systems*, pages 7800–7811, 2019.

Supplementary Materials for: Temporal Spike Sequence Learning via Backpropagation for Deep Spiking Neural Networks

Wenrui Zhang
University of California, Santa Barbara
Santa Barbara, CA 93106
wenruizhang@ucsb.edu

Peng Li
University of California, Santa Barbara
Santa Barbara, CA 93106
lip@ucsb.edu

1 Full Derivation of TSSL-BP

1.1 Forward Pass

As shown in Figure 1 of the main manuscript, we denote the presynaptic weights by $\mathbf{W}^{(l)} = [\mathbf{w}_1^{(l)}, \dots, \mathbf{w}_{N_l}^{(l)}]^T$, PSCs from neurons in layer $l-1$ by $\mathbf{a}^{(l-1)}[t] = [a_1^{(l-1)}[t], \dots, a_{N_{l-1}}^{(l-1)}[t]]$, spike trains output of the $l-1$ layer by $\mathbf{s}^{(l-1)}[t] = [s_1^{(l-1)}[t], \dots, s_{N_{l-1}}^{(l-1)}[t]]$, membrane potentials and the corresponding output spike trains of the l layer neurons respectively by $\mathbf{u}^{(l)}[t] = [u_1^{(l)}[t], \dots, u_{N_l}^{(l)}[t]]$ and $\mathbf{s}^{(l)}[t] = [s_1^{(l)}[t], \dots, s_{N_l}^{(l)}[t]]$, where variables associated with neurons in the layer l have l as the superscript.

The forward propagation between the two layers is described as

$$\begin{aligned} \mathbf{a}^{(l-1)}[t] &= (\epsilon * \mathbf{s}^{(l-1)})[t] \\ \mathbf{u}^{(l)}[t] &= \theta_\tau \mathbf{u}^{(l)}[t-1] + \mathbf{W}^{(l)} \mathbf{a}^{(l-1)}[t] + (\nu * \mathbf{s}^{(l)})[t] \\ \mathbf{s}^{(l)}[t] &= H(\mathbf{u}^{(l)}[t] - V_{th}). \end{aligned} \quad (1)$$

1.2 The Loss Function

The desired and the actual spike trains in the output layer are denoted by $\mathbf{d} = [\mathbf{d}[t_0], \dots, \mathbf{d}[t_{N_t}]]$ and $\mathbf{s} = [\mathbf{s}[t_0], \dots, \mathbf{s}[t_{N_t}]]$ where N_t is the number of the considered time steps, $\mathbf{d}[t]$ and $\mathbf{s}[t]$ the desired and actual firing events for all output neurons at time t , respectively.

In our experiments, the loss function L is defined by the square error for each output neuron at each time step:

$$L = \sum_{k=0}^{N_t} E[t_k] = \frac{1}{2} \sum_{k=0}^{N_t} (\mathbf{d}[t_k] - \mathbf{s}[t_k])^2 = \frac{1}{2} \|\mathbf{d} - \mathbf{s}\|_2^2, \quad (2)$$

where $E[t]$ is the error at time t . The loss can be also defined by using a kernel function [10]. In our experiments, we use the spike response kernel $\epsilon(\cdot)$, defining the error at each time step as

$$E[t] = \frac{1}{2} ((\epsilon * \mathbf{d})[t] - (\epsilon * \mathbf{s})[t])^2 = \frac{1}{2} (\mathbf{a}_d[t] - \mathbf{a}_s[t])^2. \quad (3)$$

1.3 Temporal Spike Sequence Learning via Backpropagation (TSSL-BP) Method

We adopt (3) to define the total loss

$$L = \sum_{k=0}^{N_t} E[t_k] = \frac{1}{2} \sum_{k=0}^{N_t} (\mathbf{a}_d[t_k] - \mathbf{a}_s[t_k])^2. \quad (4)$$

For the neurons in layer l , the error gradient with respect to the presynaptic weights matrix $\mathbf{W}^{(l)}$ is

$$\frac{\partial L}{\partial \mathbf{W}^{(l)}} = \sum_{k=0}^{N_t} \frac{\partial E[t_k]}{\partial \mathbf{W}^{(l)}}. \quad (5)$$

(1) reveals that the values of $\mathbf{u}^{(l)}$ at time t_k have contribution to all future fires and losses. Using the chain rule, we get

$$\frac{\partial L}{\partial \mathbf{W}^{(l)}} = \sum_{k=0}^{N_t} \sum_{m=0}^k \frac{\partial E[t_k]}{\partial \mathbf{u}^{(l)}[t_m]} \frac{\partial \mathbf{u}^{(l)}[t_m]}{\partial \mathbf{W}^{(l)}}. \quad (6)$$

By changing the order of summation, (6) can be written as

$$\frac{\partial L}{\partial \mathbf{W}^{(l)}} = \sum_{m=0}^{N_t} \frac{\partial \mathbf{u}^{(l)}[t_m]}{\partial \mathbf{W}^{(l)}} \sum_{k=m}^{N_t} \frac{\partial E[t_k]}{\partial \mathbf{u}^{(l)}[t_m]} = \sum_{m=0}^{N_t} \mathbf{a}^{(l-1)}[t_m] \sum_{k=m}^{N_t} \frac{\partial E[t_k]}{\partial \mathbf{u}^{(l)}[t_m]}. \quad (7)$$

We use δ to denote the back propagated error at time t_m as $\delta^{(l)}[t_m] = \sum_{k=m}^{N_t} \frac{\partial E[t_k]}{\partial \mathbf{u}^{(l)}[t_m]}$.

Therefore, the weights update formula (6) can be written as

$$\frac{\partial L}{\partial \mathbf{W}^{(l)}} = \sum_{m=0}^{N_t} \mathbf{a}^{(l-1)}[t_m] \delta^{(l)}[t_m]. \quad (8)$$

$\mathbf{a}^{(l-1)}[t_m]$ is analogous to the pre-activation in the traditional ANNs which can be easily obtained from (1) in the forward pass. $\delta^{(l)}[t_m]$ is considered in two cases.

[l is the output layer.] The $\delta^{(l)}[t_m]$ can be computed from

$$\delta^{(l)}[t_m] = \sum_{k=m}^{N_t} \frac{\partial E[t_k]}{\partial \mathbf{a}^{(l)}[t_k]} \frac{\partial \mathbf{a}^{(l)}[t_k]}{\partial \mathbf{u}^{(l)}[t_m]}. \quad (9)$$

From (4), the first term of (9) is given by

$$\frac{\partial E[t_k]}{\partial \mathbf{a}^{(l)}[t_k]} = \frac{1}{2} \frac{\partial (\mathbf{a}_d[t_k] - \mathbf{a}^{(l)}[t_k])^2}{\partial \mathbf{a}^{(l)}[t_k]} = \mathbf{a}^{(l)}[t_k] - \mathbf{a}_d[t_k]. \quad (10)$$

[l is a hidden layer.] $\delta^{(l)}[t_m]$ is derived using the chain rule and (1).

$$\delta^{(l)}[t_m] = \sum_{j=m}^{N_t} \sum_{k=m}^j \frac{\partial \mathbf{a}^{(l)}[t_k]}{\partial \mathbf{u}^{(l)}[t_m]} \left(\frac{\partial \mathbf{u}^{(l+1)}[t_k]}{\partial \mathbf{a}^{(l)}[t_k]} \frac{\partial E[t_j]}{\partial \mathbf{u}^{(l+1)}[t_k]} \right). \quad (11)$$

It is obtained from the fact that membrane potentials $\mathbf{u}^{(l)}$ of the neurons in layer l influence their (unweighted) corresponding postsynaptic currents (PSCs) $\mathbf{a}^{(l)}$ through fired spikes, and $\mathbf{a}^{(l)}$ further affect the membrane potentials $\mathbf{u}^{(l+1)}$ in the next layer. By changing the order of summation, maps

the error δ from layer $l + 1$ to layer l .

$$\begin{aligned}
\delta^{(l)}[t_m] &= \sum_{k=m}^{N_t} \frac{\partial \mathbf{a}^{(l)}[t_k]}{\partial \mathbf{u}^{(l)}[t_m]} \sum_{j=k}^{N_t} \frac{\partial \mathbf{u}^{(l+1)}[t_k]}{\partial \mathbf{a}^{(l)}[t_k]} \frac{\partial E[t_j]}{\partial \mathbf{u}^{(l+1)}[t_k]} \\
&= \sum_{k=m}^{N_t} \frac{\partial \mathbf{a}^{(l)}[t_k]}{\partial \mathbf{u}^{(l)}[t_m]} \sum_{j=k}^{N_t} \mathbf{W}^{(l+1)} \frac{\partial E[t_j]}{\partial \mathbf{u}^{(l+1)}[t_k]} \\
&= \sum_{k=m}^{N_t} \frac{\partial \mathbf{a}^{(l)}[t_k]}{\partial \mathbf{u}^{(l)}[t_m]} (\mathbf{W}^{(l+1)})^T \delta^{(l+1)}[t_k] \\
&= (\mathbf{W}^{(l+1)})^T \sum_{k=m}^{N_t} \frac{\partial \mathbf{a}^{(l)}[t_k]}{\partial \mathbf{u}^{(l)}[t_m]} \delta^{(l+1)}[t_k].
\end{aligned} \tag{12}$$

The details of the key term $\frac{\partial \mathbf{a}^{(l)}[t_k]}{\partial \mathbf{u}^{(l)}[t_m]}$ is discussed in Section 3.3.3 and 3.3.4 of the main manuscript. We'll also summarize the derivatives below.

For the key derivative $\frac{\partial a_i^{(l)}[t_k]}{\partial u_i^{(l)}[t_m]}$ ($t_k \geq t_m$) of each neuron i in layer l , we denote $\phi_i^{(l)}(t_k, t_m) = \frac{\partial a_i^{(l)}[t_k]}{\partial u_i^{(l)}[t_m]} = \phi_i^{(l)<1>}(t_k, t_m) + \phi_i^{(l)<2>}(t_k, t_m)$, where $\phi_i^{(l)<1>}(t_k, t_m)$ represents the inter-neuron dependency and $\phi_i^{(l)<2>}(t_k, t_m)$ is the intra-neuron dependency.

Assuming that the presynaptic neuron i spikes at t_m , the inter-neuron dependencies can be represented by

$$\phi_i^{(l)<1>}(t_k, t_m) = \frac{\partial a_i^{(l)}[t_k]}{\partial t_m} \frac{\partial t_m}{\partial u_i^{(l)}[t_m]}. \tag{13}$$

From (2) of the main manuscript, the first part of (13) can be calculated as

$$\frac{\partial a_i^{(l)}[t_k]}{\partial t_m} = \frac{\partial(\epsilon * s_i^{(l)}[t_m])[t_k]}{\partial t_m}. \tag{14}$$

We adopt the approach in [1, 3] to compute the second part of (11) as

$$\frac{\partial t_m}{\partial u_i^{(l)}[t_m]} = \frac{-1}{\frac{\partial u_i^{(l)}[t_m]}{\partial t_m}}, \tag{15}$$

where $\frac{\partial u_i^{(l)}[t_m]}{\partial t_m}$ is obtained by differentiating (4). In fact, (15) can be precisely derived on certain conditions.

According to the Figure 6 of the main manuscript, in the LIF model, the intra-neuron dependencies is caused by the firing-and-resetting mechanism. More precisely, $\phi_i^{(l)<2>}(t_k, t_m)$ takes this indirect intra-neuron effect on $a_i^{(l)}[t_k]$ into consideration if $\exists t_p \in (t_m, t_k)$ such that $s_i^{(l)}[t_p] = 1$ and $s_i^{(l)}[t] = 0 \forall t \in (t_m, t_p)$, i.e. no other presynaptic spike exists between t_m and t_k

$$\begin{aligned}
\phi_i^{(l)<2>}(t_k, t_m) &= \frac{\partial a_i^{(l)}[t_k]}{\partial u_i^{(l)}[t_p]} \frac{\partial u_i^{(l)}[t_p]}{\partial t_m} \frac{\partial t_m}{\partial u_i^{(l)}[t_m]} \\
&= \phi_i(t_k, t_p) \frac{\partial(\nu * s_i^{(l)}[t_m])[t_p]}{\partial t_m} \frac{\partial t_m}{\partial u_i^{(l)}[t_m]},
\end{aligned} \tag{16}$$

where $\nu(\cdot)$ is the reset kernel and $\frac{\partial t_m}{\partial u_i^{(l)}[t_m]}$ is evaluated by (15). In (16), $\phi_i^{(l)}(t_k, t_p)$ would have been already computed during the backpropagation process since t_p is a presynaptic firing time after t_m .

To sum it up, we obtain the derivative of loss with respect to weight according to TSSL-BP method as follows:

$$\begin{aligned}
\frac{\partial L}{\partial \mathbf{W}^{(l)}} &= \sum_{m=0}^{N_t} \mathbf{a}^{(l-1)}[t_m] \boldsymbol{\delta}^{(l)}[t_m], \\
\boldsymbol{\delta}^{(l)}[t_m] &= \begin{cases} \sum_{k=m}^{N_t} (\mathbf{a}^{(l)}[t_k] - \mathbf{a} \mathbf{a}[t_k]) \phi_i^{(l)}(t_k, t_m) & \text{for output layer,} \\ (\mathbf{W}^{(l+1)})^T \sum_{k=m}^{N_t} \phi_i^{(l)}(t_k, t_m) \boldsymbol{\delta}^{(l+1)}[t_k] & \text{for hidden layers,} \end{cases} \\
\phi_i^{(l)}(t_k, t_m) &= \begin{cases} 0 & s_i^{(l)}[t_m] = 0, s_i^{(l)}[t_p] = 0 \forall t_p \in (t_m, t_k), \\ \frac{\partial a_i^{(l)}[t_k]}{\partial t_m} \frac{\partial t_m}{\partial u_i^{(l)}[t_m]} & s_i^{(l)}[t_m] = 1, s_i^{(l)}[t_p] = 0 \forall t_p \in (t_m, t_k), \\ \frac{\partial a_i^{(l)}[t_k]}{\partial t_m} \frac{\partial t_m}{\partial u_i^{(l)}[t_m]} + \phi_i^{(l)<2>}(t_k, t_m) & s_i^{(l)}[t_m] = 1, \exists t_p \text{ such that } s_i^{(l)}[t_p] = 1, s_i^{(l)}[t] = 0 \forall t \in (t_m, t_p), \end{cases} \tag{17}
\end{aligned}$$

where $s_i^{(l)}[t]$ is the firing function described in (5) of the main manuscript and t_p is an arbitrary time between t_m and t_k .

2 Experiments and Results

2.1 Experimental Settings

All reported experiments are conducted on an NVIDIA Titan XP GPU. The implementation of TSSL-BP is on the Pytorch framework [9]. The experimented SNNs are based on the LIF model described in (4) of the main manuscript. The simulation step size is set to 1 ms. Only a few time steps are used to demonstrate low-latency spiking neural computation. The parameters like thresholds and learning rates are empirically tuned. Table 1 lists the typical constant values adopted in our experiments. For the time constant, we vary the membrane time constant from 2ms to 16ms. The same performance level has been observed. This indicates that the proposed method can train SNNs with dynamical behaviors across different timescales and the empirically observed results are not very sensitive to the choice of membrane time constant. No axon and synaptic delay or refractory period is used nor is normalization. Dropout is only applied for the experiments on CIFAR10. Adam [4] is adopted as the optimizer. The network models we train or compare with are either fully connected feedforward networks or convolutional neural networks (CNNs). The mean and standard deviation (stddev) of the accuracy reported are obtained by repeating the experiments five times.

Table 1: Parameters settings.

Parameter	Value	Parameter	Value
simulation step size	1 ms	Learning Rate η	0.005
Time Constant of Membrane Voltage τ_m	4 ms	Time Constant of Synapse τ_s	2 ms
Threshold V_{th}	1 mV	Batch Size	50

2.2 Input Encoding

For non-spiking datasets such as static images, the most common preprocessing is to use rate coding to convert static real-valued inputs to spiking inputs. However, this requires many time steps for coding the inputs to guarantee good performance. For static images, we directly convert the raw pixel densities into real-valued spike current inputs within a short time window. While for the neuromorphic datasets that originally contain spikes, we still use the spikes as inputs in our experiments.

2.3 Handling of Practical Issues

Two practical circumstances need to be taken into consideration as for other spike-time based BP methods like SpikeProp [1, 2]. First, when a spike is produced by the membrane potential $u[t]$ that barely reaches the threshold, the derivative of $u[t]$ w.r.t time is very small. Numerically, this can make (15) large and result in an undesirable large weight update. To mitigate, we set a bound for this

derivative. Second, absence of firing activities in spiking neurons due to low initial weight values block backpropagation through these neurons. We use a warm-up mechanism to bring up the firing activity of the network before applying the BP method. In the warm-up mechanism, we detect the firing events of each neuron. If there's at least one spike within a certain time window, TSSL-BP is applied directly. Otherwise, warm-up is applied, which uses the continuous sigmoid function of membrane potential to approximate the activation function so that the error can be propagated back even when there is no spike.

2.4 Selection of the Desired Output Spike Patterns

The desired output spike trains (labels) for different classes are manually selected without much optimization effort. In the experiments with 5 time steps, we set two fixed sequences [0, 1, 0, 1, 1] and [0, 0, 0, 0, 0] where 1 represents a spike and 0 means no spike at a given time step. We adopted a simple scheme: the number of output neurons is same as the number of classes. For each class, the first sequence is chosen to be the target of one (distinct) neuron corresponding to the class, and the second sequence is targeted for all other output neurons.

2.5 Datasets

2.5.1 MNIST

The MNIST [6] digit dataset consists of 60,000 samples for training and 10,000 for testing, each of which is a 28×28 grayscale image. Each pixel value of an MNIST image is converted into a real-valued input current. For the fully connected feedforward networks, the inputs are encoded from each $28 \times 28 \times N_t$ image into a 2D $784 \times N_t$ matrix where N_t is the simulation time steps. Each input sample is normalized to the same mean and standard deviation. No data augmentation is applied in our experiments.

2.5.2 N-MNIST

The N-MNIST dataset [8] is a neuromorphic version of the MNIST dataset generated by tilting a Dynamic Vision Sensor (DVS) [7] in front of static digit images on a computer monitor. The movement induced pixel intensity changes at each location are encoded as spike trains. Since the intensity can either increase or decrease, two kinds of ON- and OFF-events spike events are recorded. Due to the relative shifts of each image, an image size of 34×34 is produced. Each sample of the N-MNIST is a spatio-temporal pattern with $34 \times 34 \times 2$ spike sequences lasting for $300ms$ with the resolution of $1\mu s$. It means there are 300000 time steps in the original N-MNIST dataset. In our experiments, we reduce the time resolution of the N-MNIST samples by 3000 times to speed up the simulation. Therefore, the preprocessed samples only have about 100 time steps. We determine that a channel has a spike at a certain time step of the preprocessed sample if there's at least one spike among the corresponding 3000 time steps of the original sample. We demonstrate the result of the preprocessed N-MNIST with 100 time steps in Table 2 of the main manuscript. Moreover, the TSSL-BP method can well train the network only with the first $90ms$ spike sequences of the original dataset which results in 30 time steps after preprocessing. The results are shown in Table 2 of the main manuscript with only 30 time steps which keep the high level of performance as well as significantly reduce the latency.

2.5.3 FashionMNIST

The Fashion-MNIST [11] dataset contains 28×28 grey-scale images of clothing items, meant to serve as a much more difficult drop-in replacement for the MNIST dataset. The preprocessing steps are the same as MNIST.

2.5.4 CIFAR-10

The CIFAR-10 [5] dataset contains 60,000 32×32 color images in 10 different types of objects. There are 50,000 training images and 10,000 testing images. The pixel intensity of each channel is converted into a real-valued input. Similar to what are commonly adopted for preprocessing, the dataset is normalized, and random cropping and horizontal flipping are applied for data augmentation. In addition, dropout layers with a rate of 0.2 are also applied during the training of CIFAR10.

References

- [1] Sander M Bohte, Joost N Kok, and Han La Poutre. Error-backpropagation in temporally encoded networks of spiking neurons. *Neurocomputing*, 48(1-4):17–37, 2002.
- [2] Olaf Booij and Hieu tat Nguyen. A gradient descent rule for spiking neurons emitting multiple spikes. *Information Processing Letters*, 95(6):552–558, 2005.
- [3] Samanwoy Ghosh-Dastidar and Hojjat Adeli. A new supervised learning algorithm for multiple spiking neural networks with application in epilepsy and seizure detection. *Neural networks*, 22(10):1419–1431, 2009.
- [4] Diederik P Kingma and Jimmy Ba. Adam: A method for stochastic optimization. *arXiv preprint arXiv:1412.6980*, 2014.
- [5] Alex Krizhevsky, Vinod Nair, and Geoffrey Hinton. The cifar-10 dataset. *online: <http://www.cs.toronto.edu/kriz/cifar.html>*, 2014.
- [6] Yann LeCun, Léon Bottou, Yoshua Bengio, and Patrick Haffner. Gradient-based learning applied to document recognition. *Proceedings of the IEEE*, 86(11):2278–2324, 1998.
- [7] Patrick Lichtsteiner, Christoph Posch, and Tobi Delbruck. A 128×128 120 db $15\mu\text{s}$ latency asynchronous temporal contrast vision sensor. *IEEE journal of solid-state circuits*, 43(2):566–576, 2008.
- [8] Garrick Orchard, Ajinkya Jayawant, Gregory K Cohen, and Nitish Thakor. Converting static image datasets to spiking neuromorphic datasets using saccades. *Frontiers in neuroscience*, 9:437, 2015.
- [9] Adam Paszke, Sam Gross, Francisco Massa, Adam Lerer, James Bradbury, Gregory Chanan, Trevor Killeen, Zeming Lin, Natalia Gimelshein, Luca Antiga, Alban Desmaison, Andreas Kopf, Edward Yang, Zachary DeVito, Martin Raison, Alykhan Tejani, Sasank Chilamkurthy, Benoit Steiner, Lu Fang, Junjie Bai, and Soumith Chintala. Pytorch: An imperative style, high-performance deep learning library. In *Advances in Neural Information Processing Systems 32*, pages 8024–8035. Curran Associates, Inc., 2019.
- [10] Sumit Bam Shrestha and Garrick Orchard. Slayer: Spike layer error reassignment in time. In *Advances in Neural Information Processing Systems*, pages 1412–1421, 2018.
- [11] Han Xiao, Kashif Rasul, and Roland Vollgraf. Fashion-mnist: a novel image dataset for benchmarking machine learning algorithms. *arXiv preprint arXiv:1708.07747*, 2017.